TABLE S1 Cryo-EM data collection and refinement statistics.

	OS	OS-553-49	Apo-S D614G	S-553-15			S-553-60		
	Trimer	Monomer	Trimer	Dimer of trimer	Trimer	NR15	1-up trimer	2-up trimer	NR60
Data collection and processing									
Magnification	81,000		81000	81,000			105,000		
Voltage (kV)	300		300	300			300		
Total dose (e–/Å^2)	58		58	61			60		
Defocus range (μm)	-1.2 to -2.5		-1.2 to -2.5	-1.2 to -2.5			-1.2 to -2.5		
Pixel size (Å)	1.064		1.064	1.07			0.82		
Symmetry imposed	C1		C1	C1			C1		
Final particles (no.)	128,589	597,461	2,001,157	188,942	377,884	199,441	88,701	99,762	88,701
Map resolution (Å)	3.40	4.06	2.70	4.47	3.45	3.80	3.25	3.25	3.35
Refinement									
R.m.s. deviations									
Bond lengths (Å)	0.002	0.001	0.003	0.002	0.002	0.003	0.002	0.002	0.002
Bond angles (°)	0.615	0.398	0.680	0.437	0.535	0.695	0.406	0.429	0.458
Validation									
MolProbity score	2.45	2.45	2.35	2.17	2.23	2.64	2.10	2.24	2.29
Clashscore	7.53	10.22	6.44	5.82	5.80	6.92	6.56	7.05	6.74
Rotamer outlier (%)	5.36	3.78	5.57	3.89	4.31	8.82	4.23	4.57	4.60
Ramachandran plot									
Favored (%)	92.17	92.04	93.41	93.93	93.46	90.29	96.19	95.01	93.67
Allowed (%)	7.83	7.96	6.59	6.06	6.54	9.71	3.81	4.99	6.33
Disallowed (%)	0.00	0.00	0.00	0.01	0.00	0.00	0.00	0.00	0.00
EMDB	32901	32651	32902	32638	32639	32641	32646	32647	32648
PDB	7WZ1	7WOG	7WZ2	7WO4	7WO5	7WO7	7WOA	7WOB	7WOC

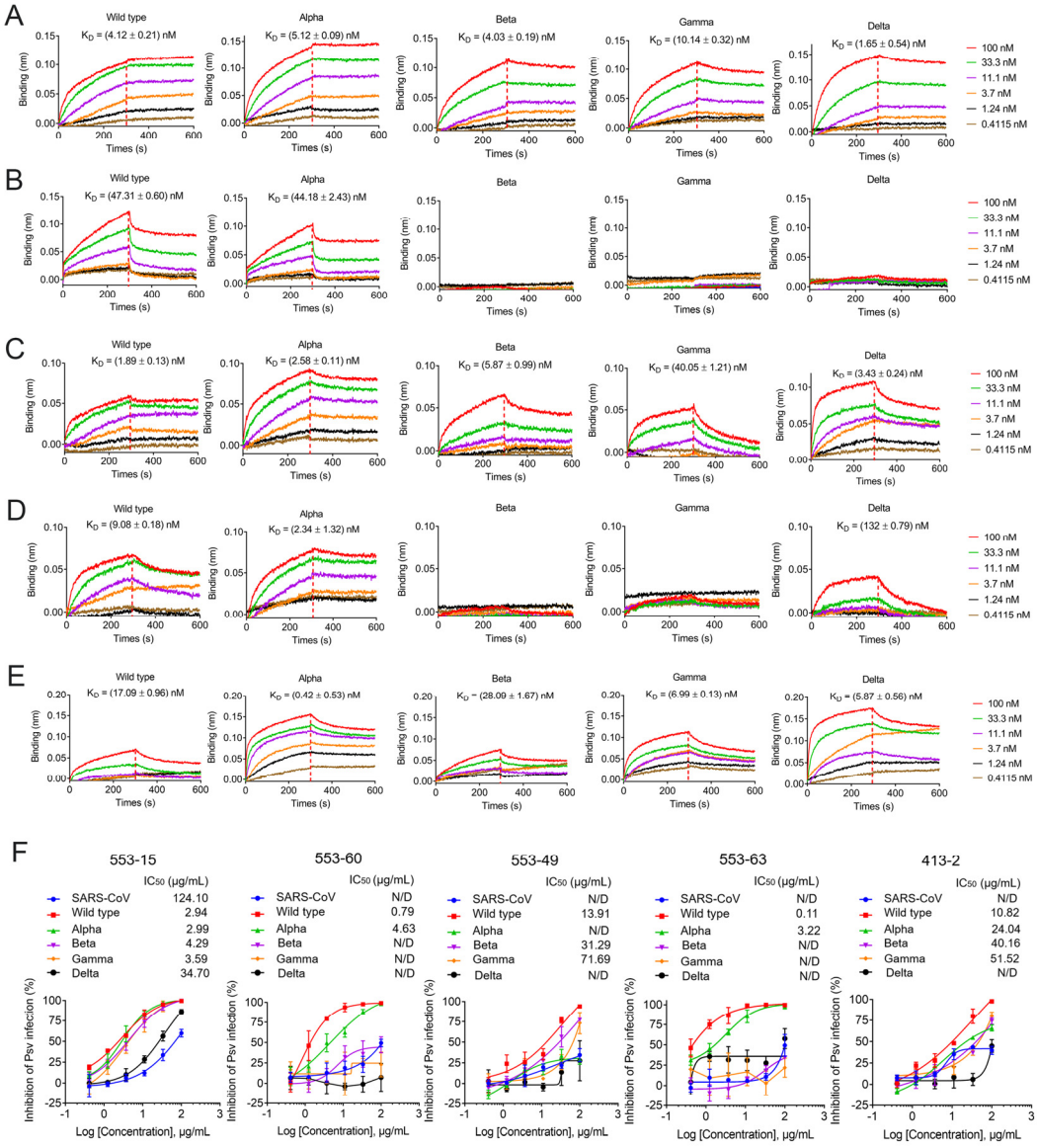

FIG S1 Accommodation of monoclonal antibodies to SARS-CoV-2 VOCs. (A-E) BLI sensorgrams and kinetics of monoclonal antibodies binding to spike protein of SARS-CoV-2 variants including: 553-15 (A), 553-60 (B), 553-49(C), 553-63 (D) and 413-2 (E). (F) Neutralizing activity of IgG against SARS-CoV-2, SARS-CoV-2 variants (Alpha, Beta, Gamma and Delta), and SARS-CoV pseudoviruses (PSV). Data are shown as mean±SEM. N/D, not detected.

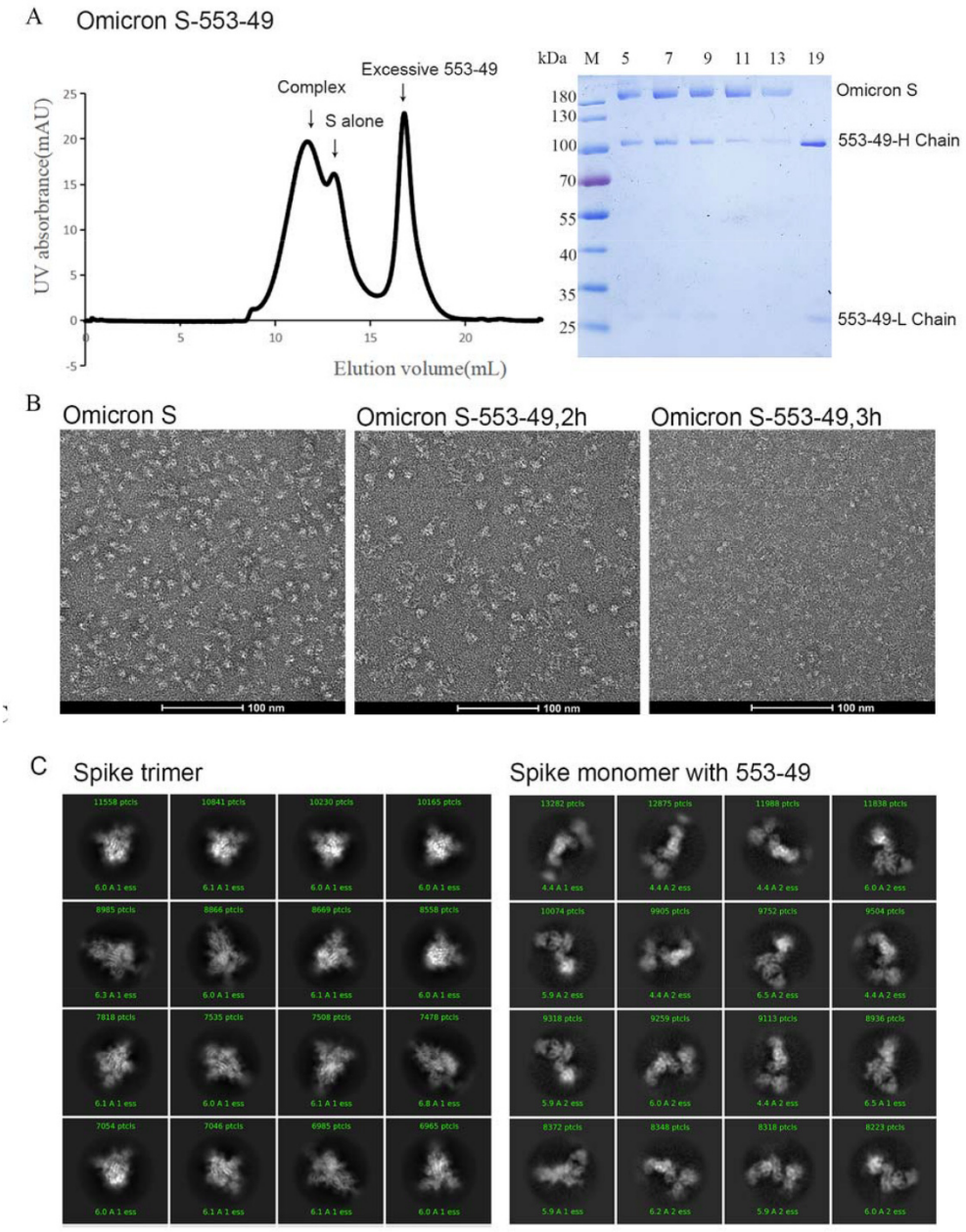

FIG S2 IgG 553-49 binds Omicron S trimer and disassembles it. (A) Purification of Omicron S-553-49 (OS-553-49) complex. The gel-filtration curve showed that 553-49 and S protein can form complex. (B) Negative stain images of OS-553-49 complex, showing that incubating Omicron S with 553-49 induced S trimer disassembling. (C) The 2D classification result of cryo-EM data collected using complex incubated for 1.5h. Two major classes were classified: the S trimer (left) and the S monomer with 553-49 (right).

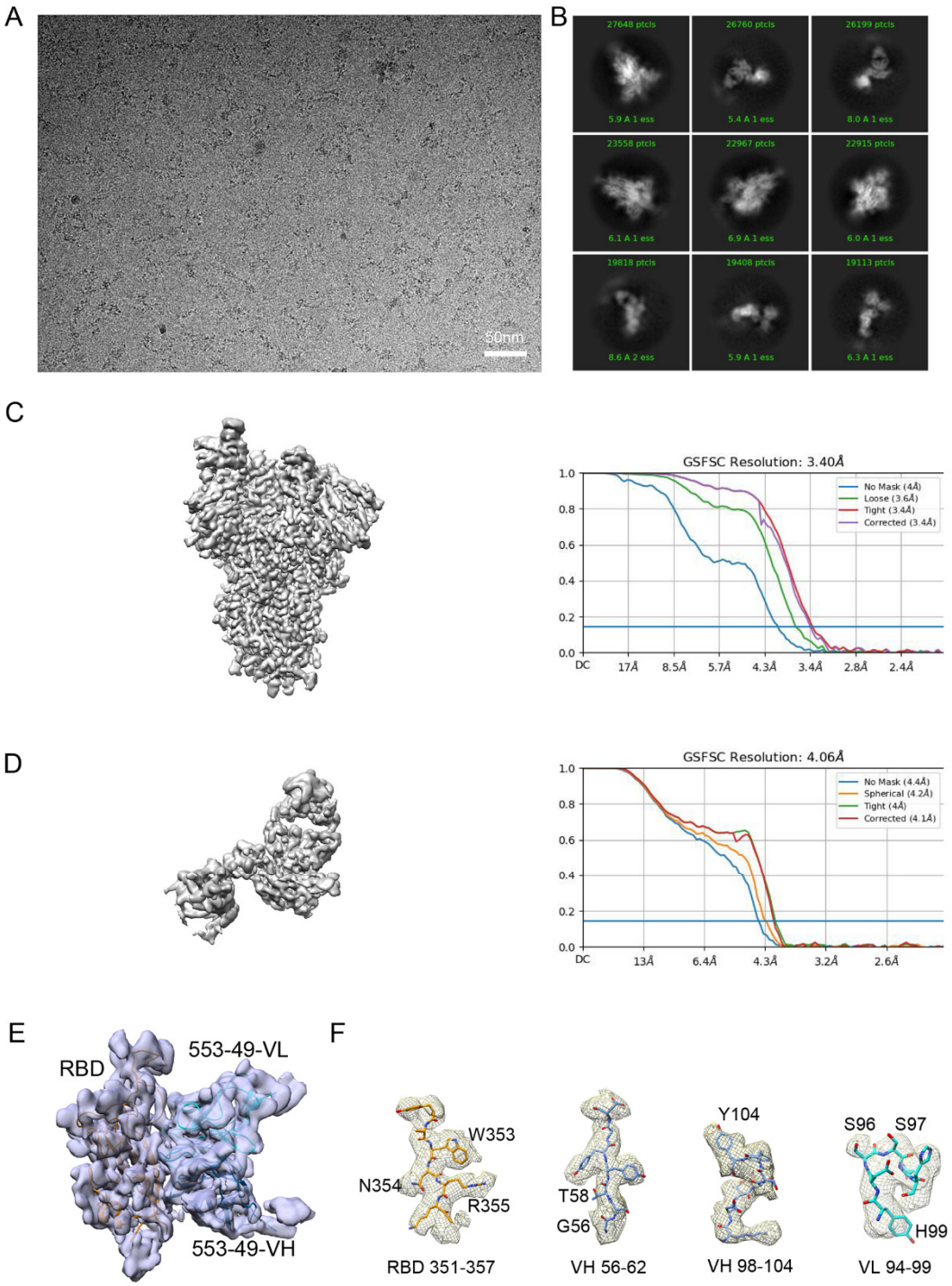

FIG S3 Cryo-EM data processing of SARS-CoV-2 Omicron S in complex with 553-49 (OS-553-49). (A) Representative electron micrograph of OS-553-49. (B) 2D classification result of OS-553-49. (C) The reconstruction map of Omicron S trimer and its gold-standard FSC curve from cryoSPARC. (D) The reconstruction map of OS-553-49 and its gold-standard FSC curve from cryoSPARC. (E) Cryo-EM map of RBD-553-49. (F) Representative density maps of residues around the interface.

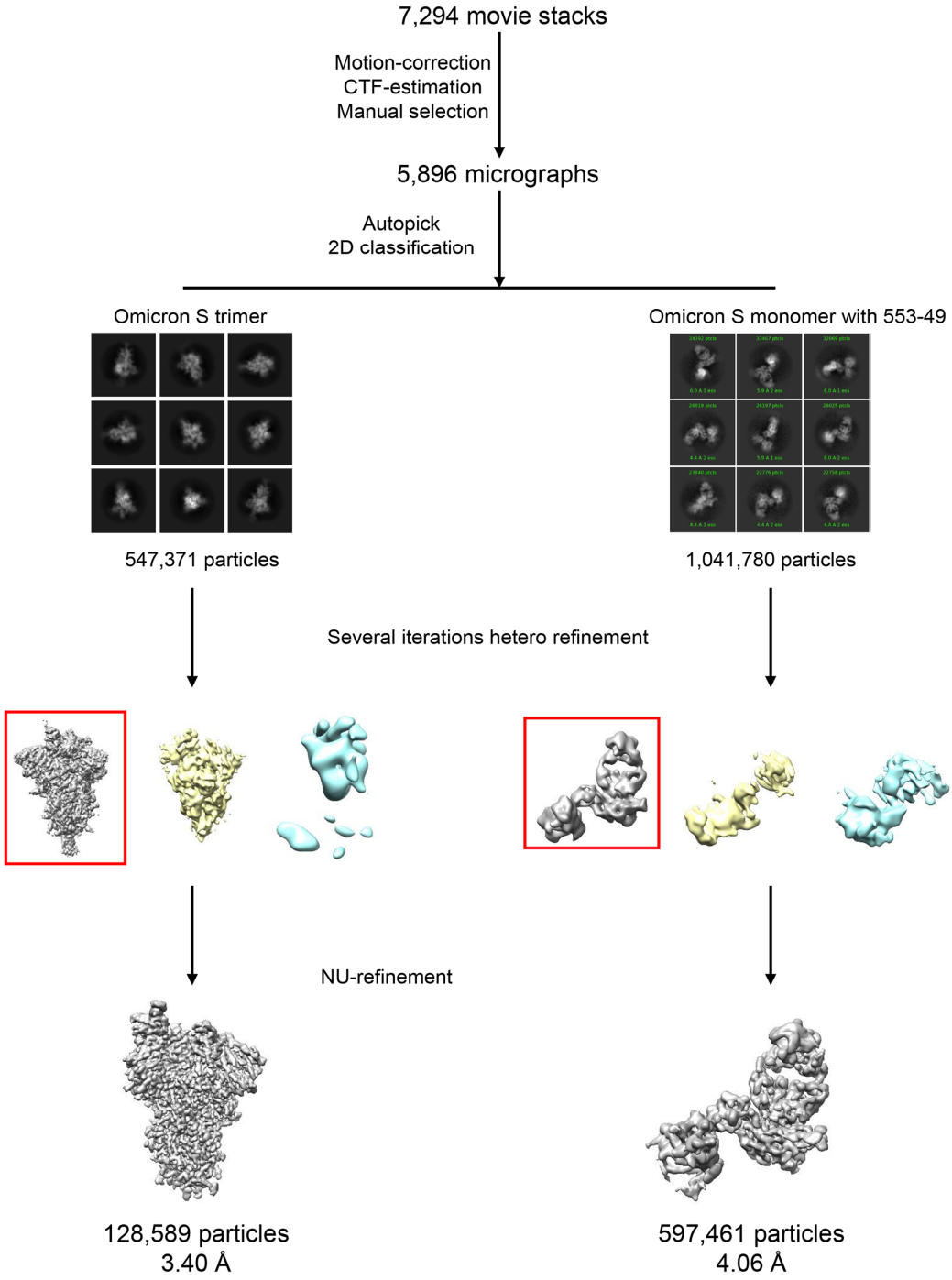

FIG S4 Data processing flowchart of Omicron S trimer and OS-553-49.

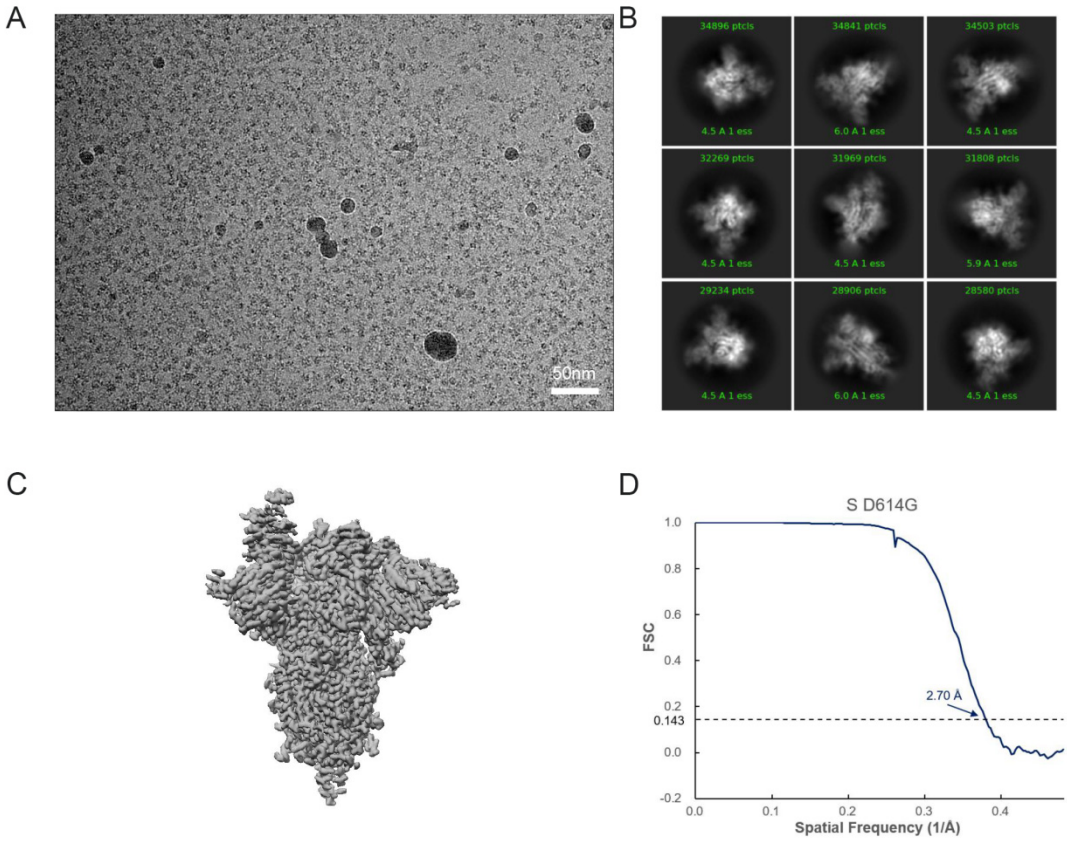

FIG S5 Cryo-EM data processing of SARS-CoV-2 D614G S. (A) Representative electron micrograph of SARS-CoV-2 S. (B) 2D classification results of SARS-CoV-2 S. (C) The reconstruction map of SARS-CoV-2 S. (D) Gold-standard FSC curves for this structure. The 0.143 cut-off is indicated by a horizontal dashed line.

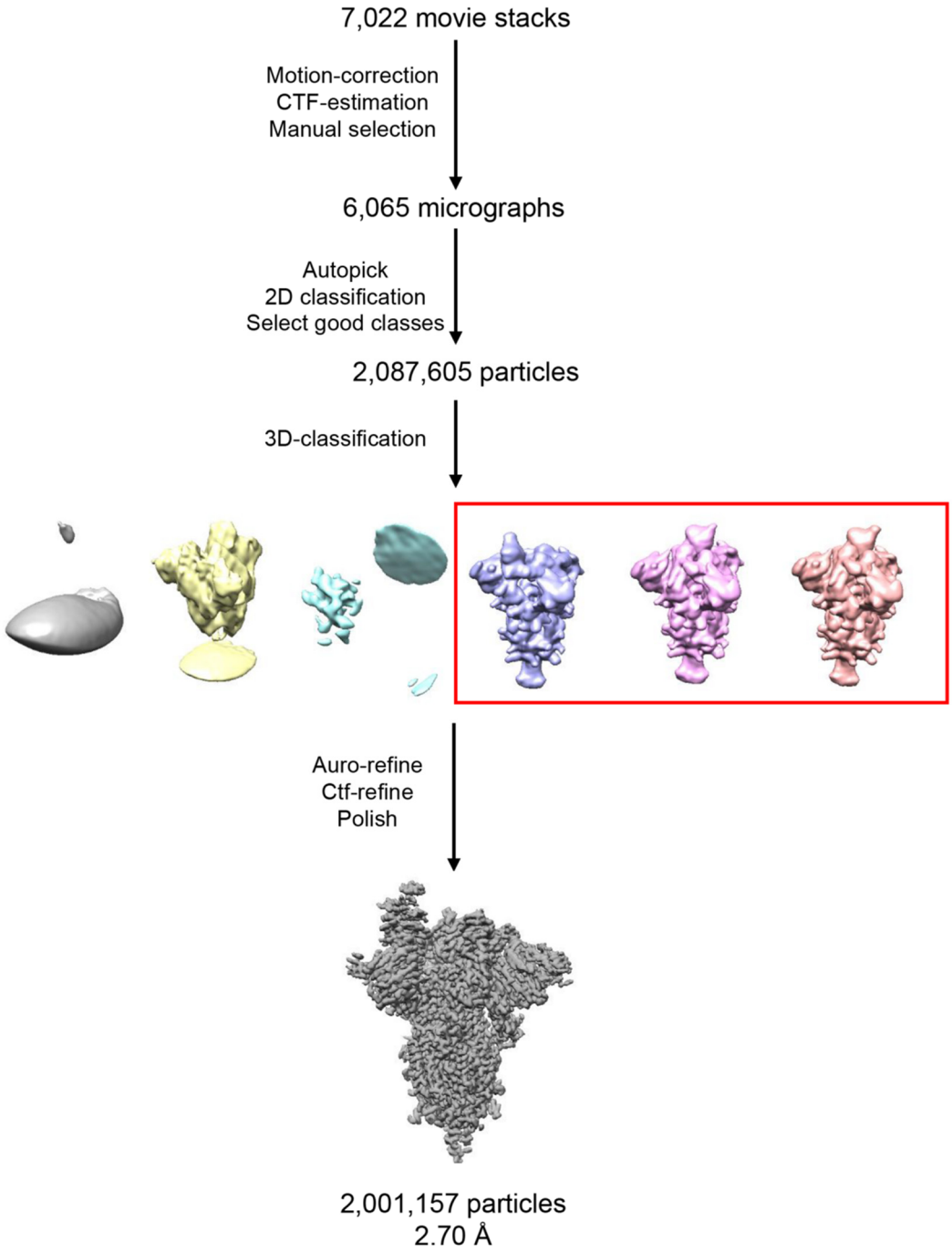

FIG S6 Data processing flowchart of SARS-CoV-2 D614G apo S trimer.

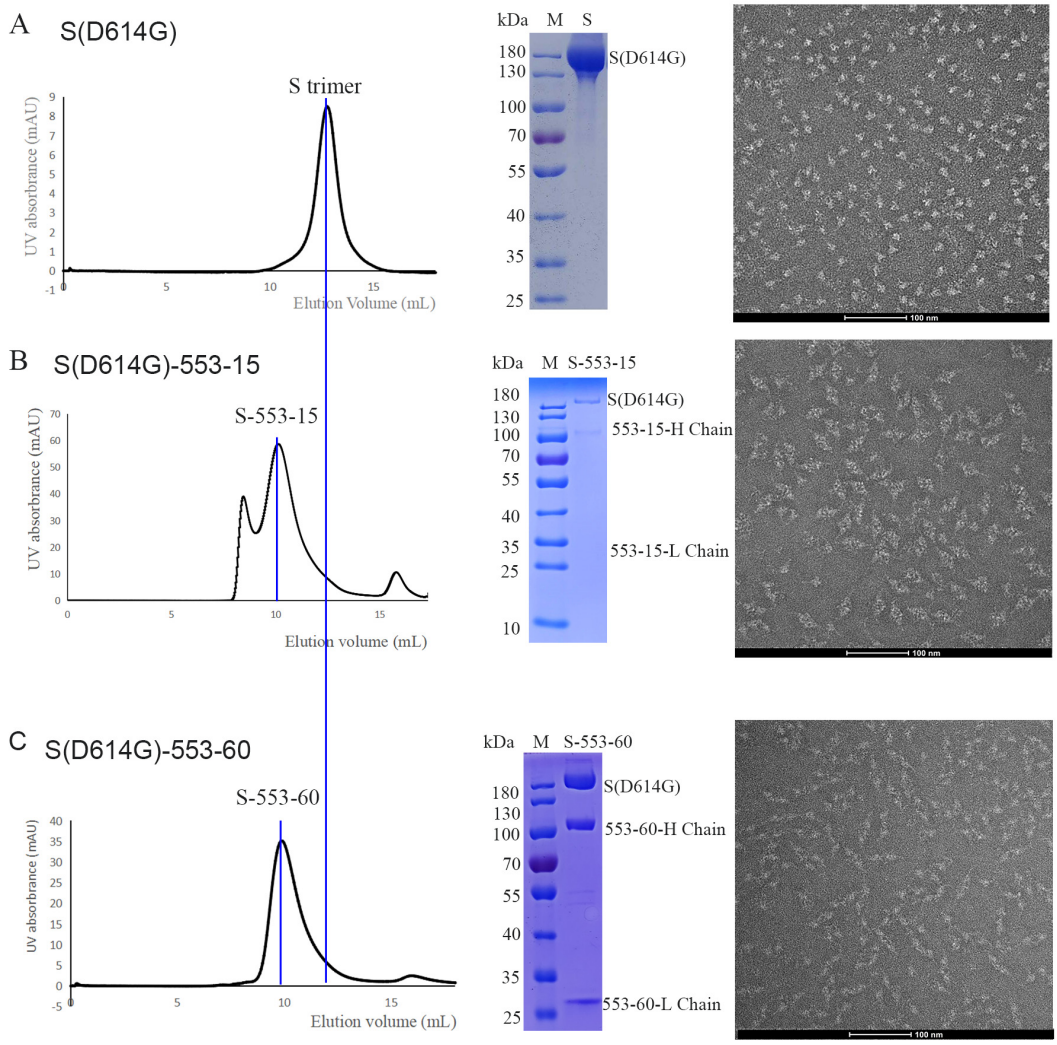

FIG S7 Sample purification. (A-B) Purification and negative stain images of S and S-553-15 complex. (C) Purification and negative stain images of S-553-60 complex. The vertical blue lines marked the peak fraction that was imaged in the gels. The negative stain images show that binding of 553-15 and 553-60 induced S trimer crosslinking of spike trimers.

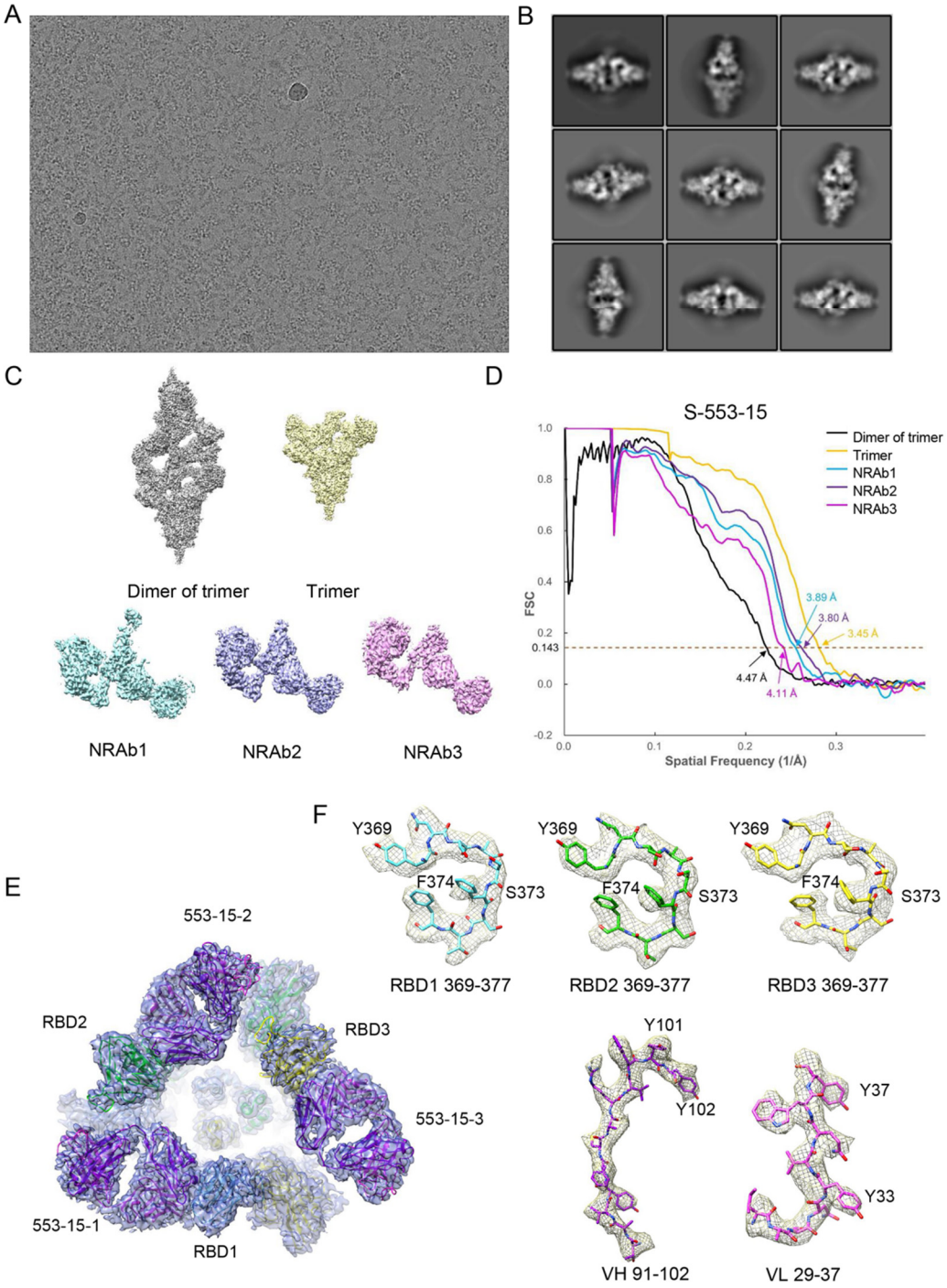

FIG S8 Cryo-EM data processing of SARS-CoV-2 D614G S complexed with 553-15 (S-553-15). (A) Representative electron micrograph of S-553-15. (B) 2D classification results of S-553-15. (C) The reconstruction map of dimer of trimer, trimer, and three local refinement maps. (D) Gold-standard FSC for each structure. The 0.143 cut-off is indicated by a horizontal dashed line. (E) Cryo-EM map of S-553-15 fitted with S-553-15 model. (F) Density maps of residues around the interface.

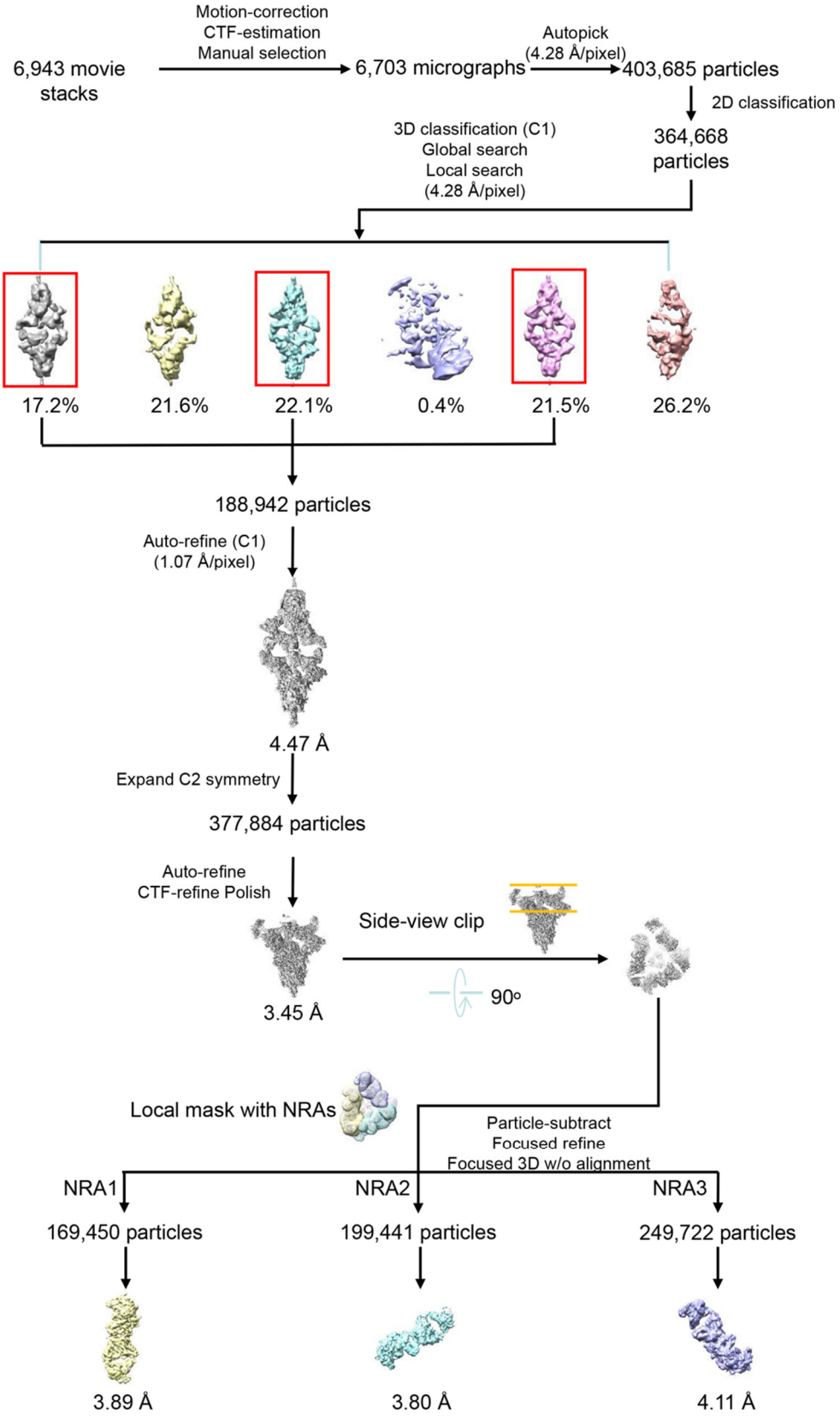

FIG S9 Data processing flowchart of S-553-15.

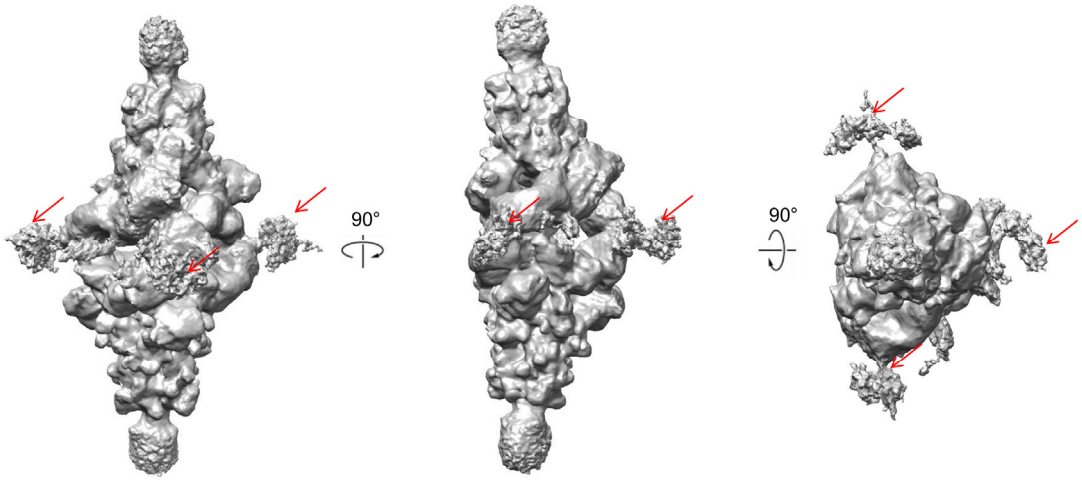

FIG S10 Fc domains of IgG 553-15 indicated in the cryo-EM map of S-553-15. Fc density is visible when map is displayed at lower contour level in Chimera.

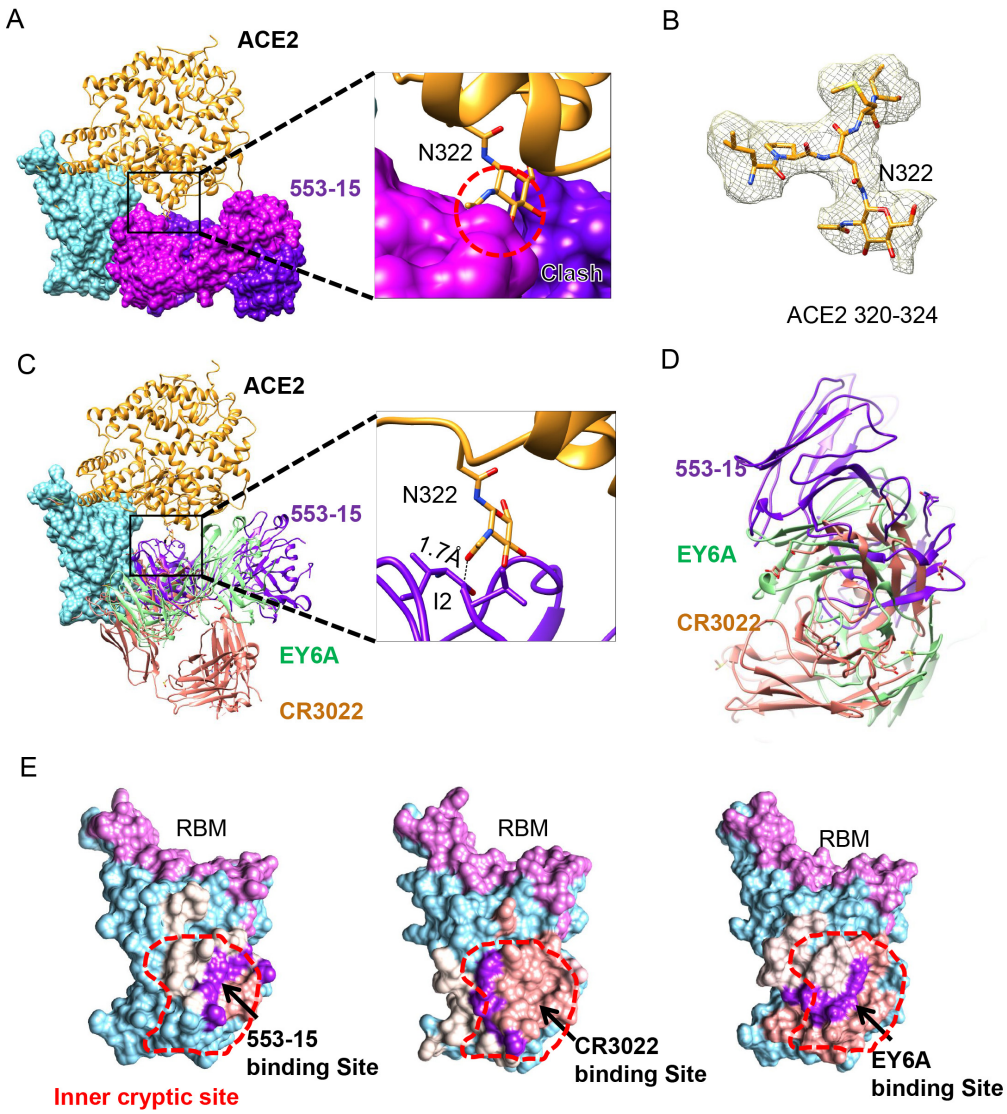

FIG S11 Comparison of 553-15, CR3022, EY6A and their epitopes on the RBDs of SARS-CoV-2 S. (A) Superposition of RBD-553-15 with RBD-ACE2 (PDBID: 6M17) showing that ACE2 would clash with 553-15. RBD and 553-15 Fab are displayed in surface. (B) Density map for N-glycan at site N322 of ACE2. (C) Comparison of Fab 553-15, EY6A and CR3022 upon binding to RBD, showing that 553-15 is closer to ACE2 N322 than EY6A (PDBID: 6ZDG) and CR3022 (PDBID: 6W41). (D) A close view of 553-15, EY6A, and CR3022 upon binding to RBD. (E) Surface representation of RBD showing the buried regions by 553-15, CR3022 and EY6A, respectively. Salmon presents VH-interacting regions, light gray presents VL-interacting regions, and purple presents the regions interacting with both VH and VL. Red dotted line indicates the inner cryptic site.

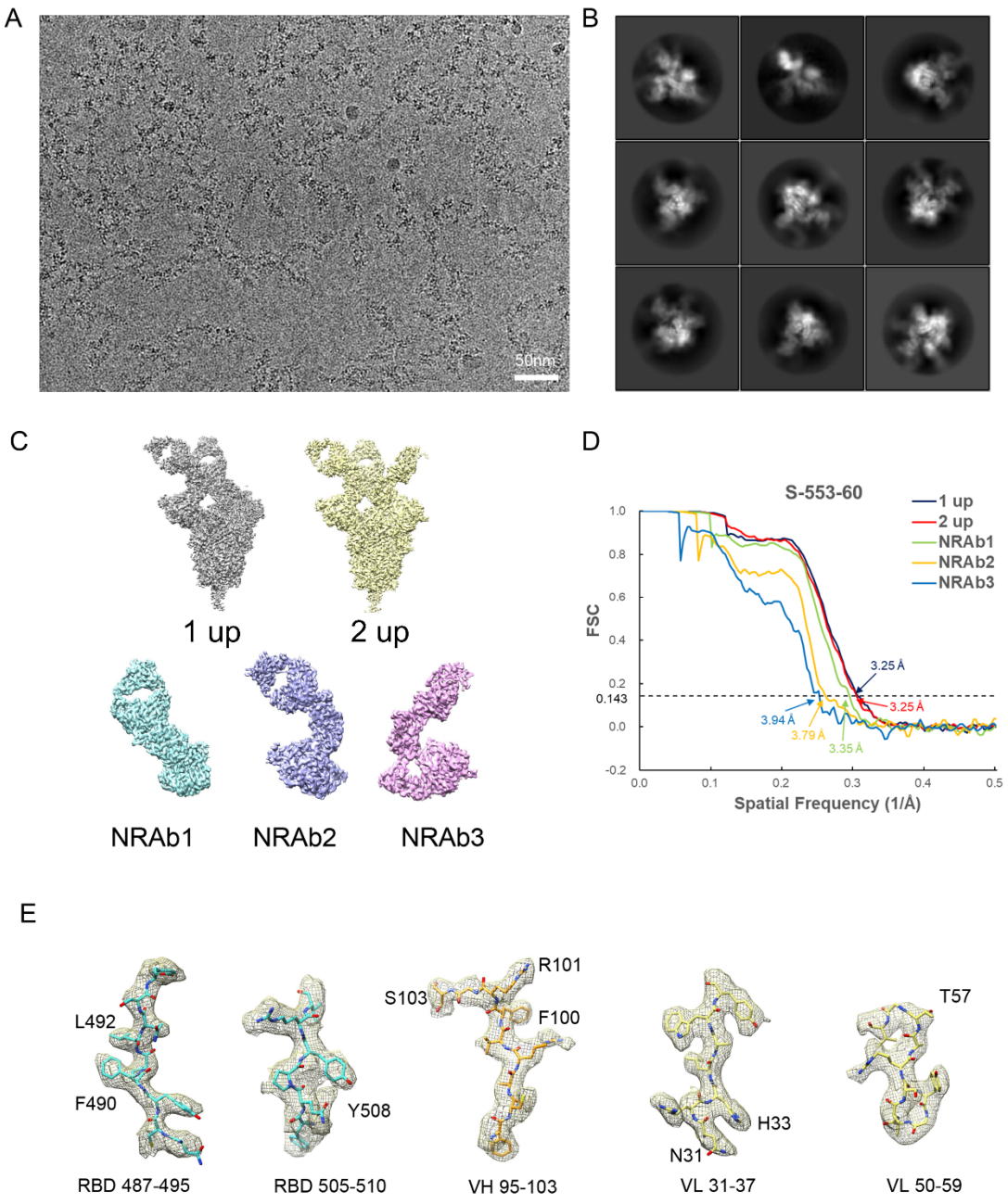

FIG S12 Cryo-EM data processing of SARS-CoV-2 D614G S complexed with 553-60 (S-553-60). (A) Representative electron micrograph of S-553-60. (B) 2D classification results of S-553-60. (C) The reconstruction maps of S-553-60 at two states and three locally refined maps. (D) Gold-standard FSC curves for each structure. The 0.143 cut-off is indicated by a horizontal dashed line. (E) Density maps of residues around the interface.

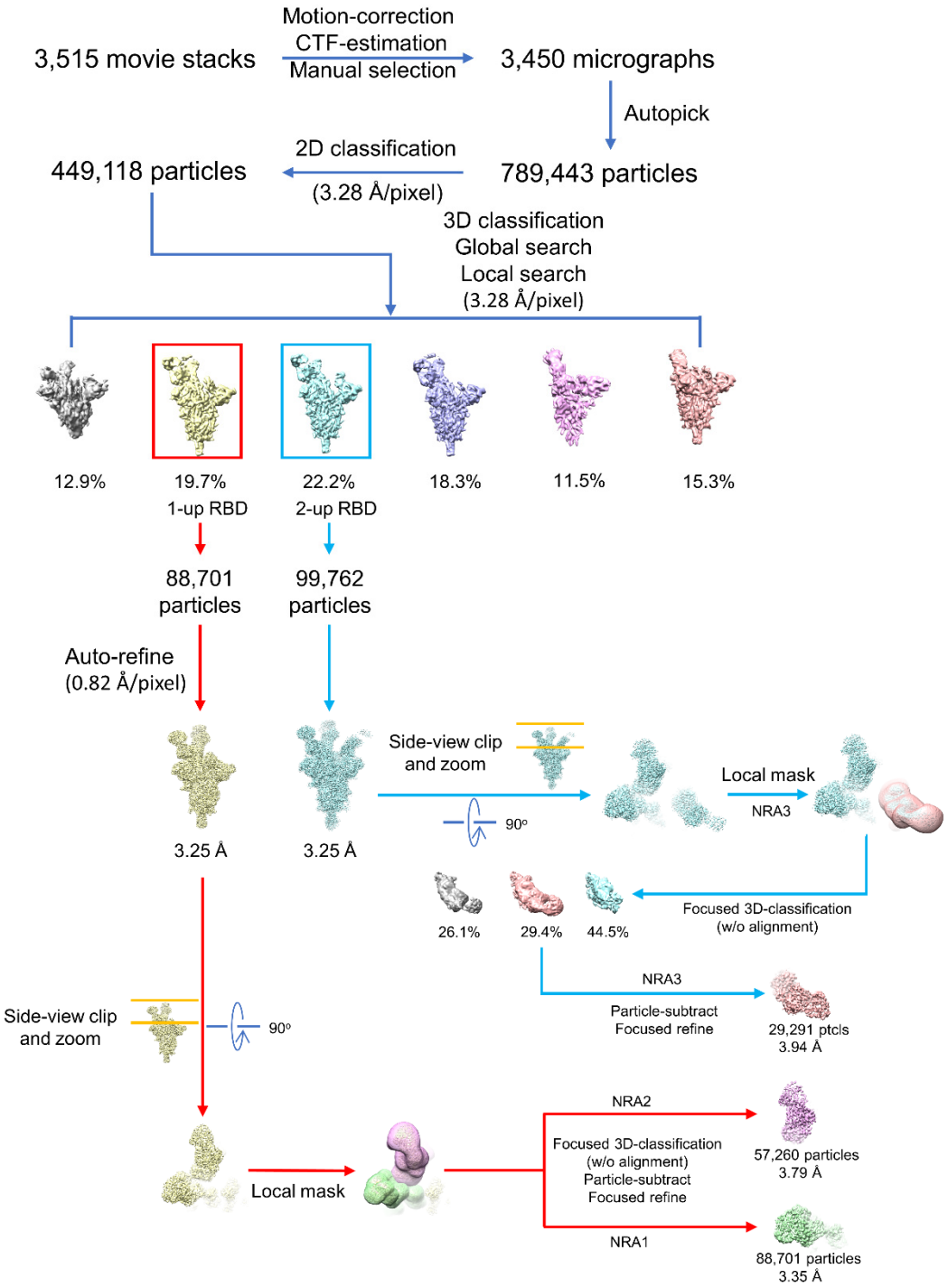

FIG S13 Data processing flowchart of S-553-60.

Movie 1 The cryo-EM structure of SARS-CoV-2 D614G S in complex with IgG 553-15. Molecular surface representation of S-553-15 complex is displayed. The dimer was formed by two S trimers with different pseudo-3-fold rotational symmetry axis. All RBDs are open.